Light scattering Q-space analysis of irregularly shaped particles

Yuli W. Heinson[1], Justin B. Maughan[1], William R. Heinson[1], Amitabha Chakrabarti[1], and Christopher M. Sorensen[1]

[1]Physics Department, Kansas State University, Manhattan, Kansas, USA

Abstract We report Q-space analysis of light scattering phase function data for irregularly shaped dust particles and of theoretical model output to describe them. This analysis involves plotting the scattered intensity versus the magnitude of the scattering wave vector $q = (4\pi/\lambda)\sin(\theta/2)$, where λ is the optical wavelength and θ is the scattering angle, on a double-logarithmic plot. In q-space all the particle shapes studied display a scattering pattern which includes a q-independent forward scattering regime; a crossover, Guinier regime when q is near the inverse size; a power law regime; and an enhanced backscattering regime. Power law exponents show a quasi-universal functionality with the internal coupling parameter ρ'. The absolute value of the exponents start from 4 when $\rho' < 1$, the diffraction limit, and decreases as ρ' increases until a constant 1.75 ± 0.25 when $\rho' \gtrsim 10$. The diffraction limit exponent implies that despite their irregular structures, all the particles studied have mass and surface scaling dimensions of $D_m = 3$ and $D_s = 2$, respectively. This is different from fractal aggregates that have a power law equal to the fractal dimension D_f because $D_f = D_m = D_s < 3$. Spheres have $D_m = 3$ and $D_s = 2$ but do not show a single power law nor the same functionality with ρ'. The results presented here imply that Q-space analysis can differentiate between spheres and these two types of irregularly shaped particles. Furthermore, they are applicable to analysis of the contribution of aerosol radiative forcing to climate change and of aerosol remote sensing data.

1. Introduction

Scattered light from spherical particles has been studied for more than 100 years and is well understood [*van de Hulst*, 1981; *Bohren and Huffman*, 1998]. However, a coherent description and understanding of light scattering by irregularly shaped particles has not been achieved. Most aerosol mass in the atmosphere, including that of entrained mineral dust, volcanic ash, and soot consists of particles with irregular shapes. The manner in which they scatter and absorb light has implications for the radiative forcing component of climate models [*Ghan and Schwartz*, 2007] and for aerosol optical remote sensing, especially satellite remote sensing [*Hoff and Christopher*, 2009]. More specifically, satellite aerosol observations use a specific angular geometry between incident solar radiation and sensor field of view; therefore, the aerosol phase function is needed to determine scattering into other directions. Similarly, calculations of aerosol radiative forcing rely on the phase function to represent the energy that is scattered toward and away from the Earth's surface. Current assumptions for aerosol phase functions range from the single-parameter Henyey-Greenstein equation [*Henyey and Greenstein*, 1941] and calculations for spherical [*Mie*, 1908] or spheroidal [*Dubovik et al.*, 2006] particles to approximations for irregularly shaped particles using composition-size-shape distributions [*Kalashnikova and Sokolik*, 2004]. Multiangle Imaging Spectroradiometer which provides independent constraints on aerosol properties has been used to study aerosols [*Kalashnikova et al.*, 2004; *Kahn and Gaitley*, 2015]. To deal with large ensembles of irregularly shaped particles in the atmosphere, a universal description of phase functions is needed that will hopefully lead toward more realistic and practical phase functions for remote sensing and radiative forcing applications.

In this paper, we apply Q-space analysis [*Sorensen and Fischbach*, 2000; *Berg et al.*, 2005; *Sorensen*, 2013b] to the angular distribution of scattered light for a wide range of irregularly shaped particles using both experimental and theoretical data produced by our group and by others. "Q-space analysis" refers to the use of q, representing the magnitude of the scattering wave vector:

$$q = 2k \sin(\theta/2) \tag{1}$$

where $k = 2\pi/\lambda$ with λ the wavelength and θ is the scattering angle. Equation (1) is well known; for a derivation see, e.g., *Sorensen* [2001]. The experimental data include 43 aerosol data sets from the Amsterdam-Granada group
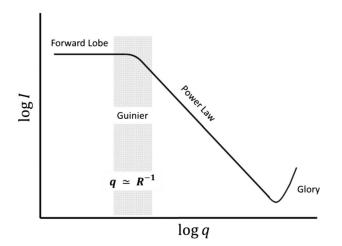
Figure 1. A generalized schematic of Q-space analysis for nonspherical particles. Scattered intensity *I* with arbitrary units (a.u.) is plotted versus *q* (cm^{-1}) on a log-log scale.

[*Munoz et al.*, 2000, 2001, 2002, 2004, 2006, 2007, 2012; *Volten et al.*, 2001, 2006; *Laan et al.*, 2009]. The Amsterdam-Granada group measured scattering matrix elements (S_{11}, S_{12}/S_{11}, S_{22}/S_{11}, S_{33}/S_{11}, S_{34}/S_{11}, S_{44}/S_{11}) as a function of angle for all the aerosols they studied. We only picked up S_{11} versus θ, the phase function. The experimental data also include our recent work on Ultrafine, Fine, and Medium Arizona Road Dust (AZRD) samples [*Wang et al.*, 2015] and the data on Ultrafine AZRD from *Curtis et al.* [2008]. The theoretical data include Gaussian random spheres and thickened percolation clusters from our group, and irregular spheres from a collaboration between our group and Zubko [*Sorensen et al.*, 2014]. Power laws with quantifiable exponents are revealed under Q-space analysis for all particles presented; thus achieving a universal description. Moreover, the exponents of the power laws are a function of the internal coupling parameter ρ' [*Heinson et al.*, 2015] that incorporates information on the particle size and composition via the refractive index:

$$\rho' = 2kR\left|\frac{m^2 - 1}{m^2 + 2}\right|, \qquad (2)$$

where R is the effective radius, e.g., volume equivalent radius of the particle, and $m = n + i\kappa$ is the particle's refractive index. We find an undeniable trend in the absolute value of the exponents with ρ'; the absolute value of the exponents is 4 when $\rho' < 1$, decreases with increasing ρ', and then reach a plateau of approximately 1.75 $\pm$ 0.25 at large ρ'.

2. Q-Space Analysis

Conventionally, observational data for the scattered intensity is plotted versus the scattering angle θ. However, we apply Q-space analysis [*Sorensen and Fischbach*, 2000; *Berg et al.*, 2005; *Sorensen*, 2013b] wherein the scattered intensity is plotted versus the magnitude of the scattering wave vector q or the dimensionless qR on a log-log scale (equivalent results; however, the latter variable eliminates the particle size dependence). Unlike plotting versus linear θ which yields no definable pattern, Q-space analysis reveals a series of regimes as a function of q common to all particle shapes. In particular, power law functionalities of the scattered intensity versus q with quantifiable exponents are uncovered. Thus, an amorphous description gives way to a quantified and specific one that can be used to describe similarities and differences between scatterings by different types of particles.

Previous work applying Q-space analysis to spheres has shown two [*Sorensen and Fischbach*, 2000; *Berg et al.*, 2005] and, when the sphere is large, three power law regimes [*Heinson et al.*, 2014] between the Guinier and enhanced backscattering regimes (see below). Soot fractal aggregates [*Sorensen*, 2001] and recent work on limited samples of dusts [*Sorensen*, 2013a; *Wang et al.*, 2015] show a single power law, distinctively different than spheres. Figure 1 shows a simple, generalized schematic of the results of Q-space analysis for irregularly shaped particles as we know it so far. A constant forward scattering lobe at small q is followed by, at larger q, a crossover, Guinier regime near $q \simeq R^{-1}$, where R is a radial dimension, a power law regime; and finally, an enhanced backscattering regime, the Glory, is sometimes observed at the largest values of q near $2k$. This description applies to spheres as well, except that the power law regime has more than a single power law as described above. These simple patterns give a unified description for all particle shapes.

3. The Internal Coupling Parameter ρ'

In recent work [*Heinson et al.*, 2015] we show that patterns revealed by Q-space analysis are better parameterized by the internal coupling parameter ρ' given in equation (2) above than by the more widely known phase shift parameter $\rho = 2kR(m - 1)$, that was used in our previous work [*Sorensen and Fischbach*, 2000; *Berg et al.*, 2005; *Sorensen*, 2013b]. The phase shift parameter ρ describes the phase difference between a beam of light traveling through the diameter of the sphere and another that travels the same distance outside the sphere. In contrast ρ' is related to the Lorentz-Lorenz factor which is directly involved in the radiative coupling between the subvolumes that comprise the particle. When the coupling is strong, the field within the particle is no longer equal to the incident field; hence, the scattering is no longer in the Rayleigh-Debye-Gans (RDG) limit which occurs at small ρ' (and ρ). When in the RDG limit, the scattering is simple diffraction from the volume of the particle, and as such, the scattered intensity is the Fourier transform of the shape of the particle, squared. This new parameter was first realized by the need for spherical particle scattering to cross over from the small particle RDG limit to large particle Fraunhofer diffraction which is described by a two-dimensional circular obstacle. Spheres that are small compared to the wavelength of light have scattered intensities given by the Rayleigh differential cross section [*Kerker*, 1969; *van de Hulst*, 1981; *Bohren and Huffman*, 1998]

$$\frac{dC_{sca,\,Ray}}{d\Omega} = k^4 R^6 \left| \frac{m^2 - 1}{m^2 + 2} \right|^2 \tag{3}$$

As spheres become very large, the scattering is described by Fraunhofer diffraction by a two-dimensional circular obstacle with forward scattering given as

$$\frac{dC_{sca}}{d\Omega}(0) = k^2 R^4 / 4 \tag{4}$$

which is well established, see, e.g., *Hecht* [2002]. The ρ' parameter is derived as the square root of the ratio between equations (3) and (4). Note that both ρ' and ρ assume a homogeneous particle with regard to the refractive index m, although we expect that, if inhomogeneous, a Maxwell-Garnet average m would make a good approximation. All the particles studied here were homogeneous or to a very good approximation.

4. Q-Space Analysis of Scattering by Aerosol Particles

4.1. Analysis of Prior Published Data Sets

The Amsterdam-Granada group has measured light scattering from various kinds of irregularly shaped aerosol particles such as feldspar, red clay, quartz, volcanic ash, and many others at wavelengths 441.6 nm and 632.8 nm [*Munoz et al.*, 2000, 2001, 2002, 2004, 2006, 2007, 2012; *Volten et al.*, 2001, 2006; *Laan et al.*, 2009]. Their volcanic ash was collected from different locations, years, and time after possible eruptions. The phase functions could not be normalized due to the lack of the exact forward and backward direction measurements. The Amsterdam-Granada group normalized all their intensities at 30°. We applied Q-space analysis to all 43 aerosol data sets available on their website as shown in Figures 2a–2i, where the scattered intensity with arbitrary units is plotted versus q (cm^{-1}). A different, arbitrary multiplication factor is applied to the intensity for each aerosol simply for clarity in the figure. Q-space analysis with its double logarithmic axes reveals that the data have a linear relationship in this space, with the fitted power law exponent values labeled on the right side of each curve. It is important to stress that in contrast to the behavior in Q-space, plotting the data with a linear abscissa representing the scattering angle θ yields nondescript, indistinguishable curves. Figure 3 [*Sorensen*, 2013b] is an example of this comparison between conventional analysis and Q-space analysis on desert dust.

The data are limited in that they do not show a constant forward scattering lobe and only some of them show a portion of a Guinier regime. This limitation is due to minimum scattering angles larger than either 3° or 5°. Consequently, neither the true forward scattering regime nor the Guinier regime is captured in the scattering data for sizes greater than $R \approx \lambda/2\theta$ (derived from the Guinier regime $q \simeq R^{-1}$, see Figure 1, and Fraunhofer diffraction, see, e.g., *Hecht* [2002]) which is ~5 microns for 3°.

The exponents for the power law regime are obtained by fitting the data after the Guinier regime, when present, and before the Glory. For example, scattering by volcanic ash from the Pinatubo volcano measured
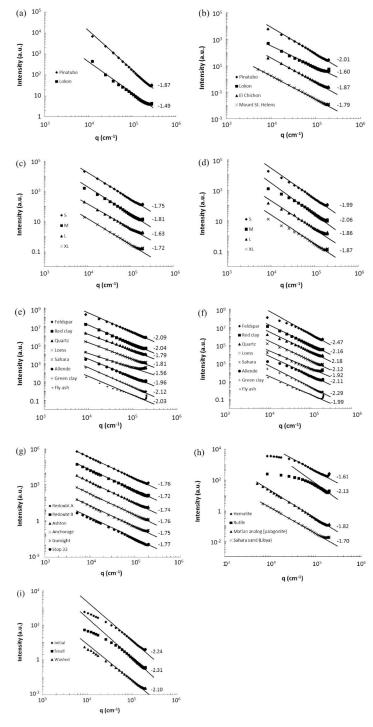
Figure 2. Scattered intensities (a.u.) (intensities have been scaled for clarity) expressed as functions of the parameter *q* (cm^{-1}), for studies of the indicated particle types, as reported by the Amsterdam-Granada group [*Munoz et al.*, 2000, 2001, 2002, 2004, 2006, 2007, 2012; *Volten et al.*, 2001, 2006; *Laan et al.*, 2009]. Lines are the power law fits proposed in this work, and the numbers to the right of the plots are the exponents of the power law. (a) Volcanic ash (Pinatubo, Lokon) measured at $\lambda = 441.6$ nm. (b) Volcanic ash (Pinatubo, Lokon, El Chichol, and Mount St. Helens) measured at $\lambda = 632.8$ nm. (c) Olivine S, Olivine M, Olivine L, and Olivine XL measured at $\lambda = 441.6$ nm. (d) Olivine S, Olivine M, Olivine L, and Olivine XL measured at $\lambda = 632.8$ nm. (e) Feldspar, Redy clay, Quartz, Loess, Sahara, Allende, Green clay, and Fly ash measured at $\lambda = 441.6$ nm. (f) Feldspar, Redy clay, Quartz, Loess, Sahara, Allende, Green clay, and Fly ash measure at $\lambda = 632.8$ nm. (g) Volcanic ash (Redoubt A, Redoubt B, Spurr Ashton, Spurr Anchorage, Spurr Gunsight, and Spurr Stop 33) measured at $\lambda = 632.8$ nm. (h) Hematite, Rutile, Martian analog (palagonite), and Sahara sand (Libya) measured at $\lambda = 632.8$ nm. (i) Forsterie initial, Forsterie small, and Forsterie washed measured at $\lambda = 632.8$ nm.
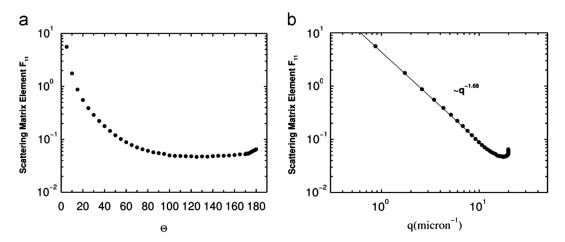
Figure 3. Comparison between conventional analysis and Q-space analysis on desert dust [*Sorensen*, 2013b]. The same data are plotted on each side of the figure. Plotting the data versus linear θ (left) yields a nondescript curve; plotting versus logarithmic *q* (right) yields an obvious straight line regime indicating a power law.

at $\lambda = 441.6$ nm obeys the power law with the exponent of -1.87 found from a fit to the data, excluding the first few points and the Glory points. The Amsterdam-Granada group provided the effective radius and the refractive index for each kind of aerosol particle, which allows us to calculate the internal coupling parameter ρ'. We noticed that the exponents evolve with increasing ρ'. The supporting information file shows ρ' and the corresponding exponent for each particle presented.

4.2. Arizona Road Dust (AZRD)

In our previous work we conducted measurements on three AZRD samples. The experimental method, the images, the Q-space analysis of AZRD, and other details are presented in *Wang et al.* [2015]. Q-space analysis on AZRD showed power laws with quantifiable exponents of -2.23, -2.17, and -2.12 for the Ultrafine, Fine, and Medium (as named by the provider, Powder Technology, Inc.) dust samples, respectively; all with uncertainties of ± 0.05 [*Wang et al.*, 2015]. The sizes of the three AZRD samples were measured via a Guinier analysis of the light scattering data, and the sizes were 2.7 μm, 5.5 μm, and 9.7 μm for the Ultrafine, Fine, and Medium dust samples, respectively [*Wang et al.*, 2015]. These sizes along with the refractive index of 1.54 [*Gorner et al.*, 1995; *Wang et al.*, 2009] were used to calculate ρ' with equation (2). Hence, ρ' increases from Ultrafine to Medium AZRD, which indicates that the exponents decrease with increasing ρ's. *Curtis et al.* [2008] conducted experiments on one AZRD sample [*Curti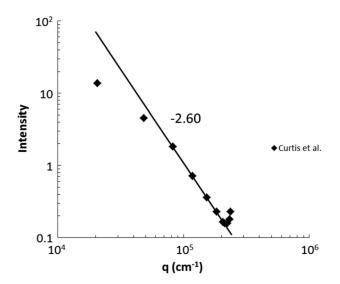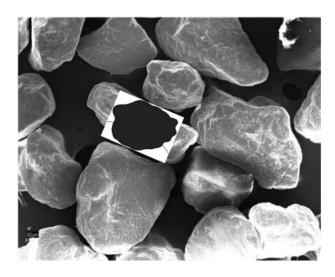s et al.*, 2008]. They used an experimental method which produced much smaller Ultrafine AZRD particles with the projected surface area weighted effective radius 0.318 μm [*Curtis et al.*, 2008]. This radius implies a Guinier regime near $q \approx 3 \times 10^4$ cm^{-1}. We extrapolated their experimental data and did Q-space analysis for q values larger than this Guinier value to find a power law with the exponent of -2.60 as shown in Figure 4.

4.3. Gaussian Random Spheres (GRSs)

Gaussian random spheres (GRSs) have been used to model many different objects from asteroids to dust and ice particles [*Muinonen*, 1998; *Muinonen and Lagerros*, 1998;

Figure 4. Q-space analysis on extrapolated AZRD data from *Curtis et al.* [2008].

Figure 5. GRS model compared to Saharan dust particles from *Munoz et al.* [2007].

Munoz et al., 2007; *Nousiainen et al.*, 2011a, 2011b]. Figure 5 shows a GRS model compared to Saharan dust (Libya) particles from *Munoz et al.* [2007]. GRSs are described by three parameters: (1) a, the mean radius, which sets the overall size of the particle; (2) σ, the relative standard deviation in the radial direction which is used as a measure of the size of fluctuations in radial directions away from the mean radius a. The standard deviation would be calculated by taking the square root of the sum of the square of the difference of the actual radii from the mean radius. The relative standard deviation is the standard deviation normalized by the mean radius; and (3) v, the power law exponent that controls the angular range of fluctuations in a tangential direction. For general descriptions of GRSs the reader is directed to *Veihelmann et al.* [2006], *Muinonen et al.* [2007], and *Nousiainen et al.* [2011b] and for a more in-depth mathematical treatment to *Lamberg et al.* [2001].

In our work recently accepted for publication [*Maughan et al.*, 2015] GRSs with $\sigma = 0.2$ and $v = 3$ were systematically studied theoretically with size parameters ranging from $ka = 10$ to 30, with a relative index of refraction, m, ranging from 1.01 to 1.5. The scattered intensity was calculated for many different orientations and then averaged using a Discrete Dipole Approximation (DDA) [*Purcell and Pennypacker*, 1973; *Draine and Flatau*, 1994; *Kalashnikova and Sokolik*, 2004]. The results show power law descriptions of the scattering in Q-space between the Guinier regime and the Glory. One example is shown in Figure 6 where $ka = 30$. The exponent for each ρ' is labeled by each plot. We noticed that exponents evolve with increasing ρ', again similar to the conclusion in section 4.1.

4.4. Thickened Percolation Clusters

We wanted an irregularly shaped particle that was not a perturbation of a sphere to mimic certain irregular aerosol found in nature [*Popovicheva et al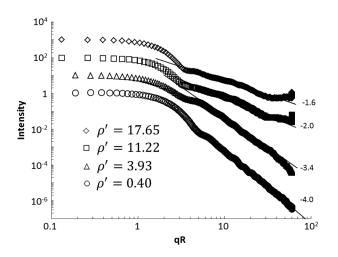.*, 2012]. Our recent work simulates three-dimensional dust agglomerate particles by using clusters made under the classical site percolation theory as a backbone. Percolation clusters are made on a square lattice that has sites randomly filled. When filled sites are neighbors, they are considered joined into a cluster. As more sites are filled, clusters become larger until one reaches the desired size and is set aside to be used as the backbone for the dust particle. Percolation clusters are described by their fractal dimension of $D_f \simeq 2.5$; therefore, to make the fractal dimension match the spatial dimension of three, the backbone cluster is then thickened by filling the neighboring sites. Figure 7 shows an example of a thickened percolation cluster.

Figure 6. Q-space analysis on GRSs with $ka = 30$, $\sigma = 0.2$, and $v = 3$. Lines are the power law fits and the numbers to the right of the plots are the exponents of the power law. A different multiplication factor is applied to the intensity for each plot to separate one from the other.
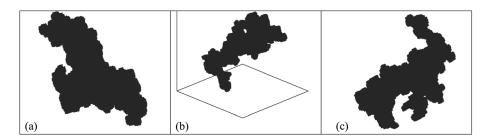
Figure 7. Thickened percolation cluster (a) side view, (b) three quarters view, and (c) top view.

The rotationally averaged scattered intensity was calculated using DDA [*Purcell and Pennypacker*, 1973; *Draine and Flatau*, 1994; *Kalashnikova and Sokolik*, 2004]. Then with the application of Q-space analysis as shown in Figure 8, power law regimes after the Guinier regime become apparent. As before, the exponents evolve with increasing ρ'.

4.5. Irregular Spheres

Zubko and colleagues [*Zubko et al.*, 2006, 2008, 2009] used DDA [*Draine and Flatau*, 1994] to calculate light scattering by four different types of irregularly shaped spheres: strongly damaged spheres, rough surface spheres, pocked spheres, and agglomerated debris particles. In collaboration with Zubko our group applied Q-space analysis and reported the results including power law exponents in *Sorensen et al.* [2014].

5. The Exponent of Q-Space Analysis as a Function ρ'

Figure 9 is a plot of the power law exponents uncovered by Q-space analysis versus the internal coupling parameter ρ' for all the irregularly shaped particles studied above. Figure 9 clearly shows an undeniable trend that as ρ' increases, the absolute value of the exponents from the power law regimes decrease, and that all the particles fall on the same trend regardless of the detail of their structure. The exponents start from 4 when ρ' is small. As ρ' increases, the exponents decrease until the trend levels off at $\rho' \gtrsim 10$ where the exponents reach a constant 1.75 ± 0.25. The supporting information file shows the ρ' values and the corresponding exponent absolute values for all the data presented in Figure 9.

In the $\rho' \rightarrow 0$ diffraction RDG limit, the power law regime, in general, obeys [*Oh and Sorensen*, 1999]

$$I(q) \sim q^{-(2D_m - D_s)} \tag{5}$$

In (5) D_m is the particle mass scaling dimension and D_s is the particle surface scaling dimension. For example, spheres have $D_m = 3$ and $D_s = 2$ to yield via (5) the Porod exponent 4 [*Porod*, 1951] when $\rho' < 1$. Although not
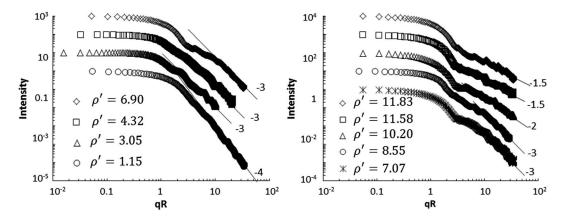

Figure 8. Q-space analysis on thickened percolation clusters. Lines are the power law fits and the numbers to the right of the plots are the exponents of the power law. A different multiplication factor is applied to the intensity for each plot for clarity.
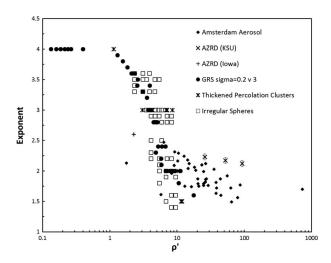
Figure 9. The exponents of the power laws versus the internal coupling parameter ρ'.

all the shapes in Figure 9 have small ρ' values, the similar trend implies that all shapes would have a power law exponent of 4 when $\rho' < 1$. If true, then all the irregular shapes studied here and displayed in Figure 9 have $D_m = 3$ and $D_s = 2$; the same as spheres, and hence do not have the fractal morphology. A corollary to this is that "regularly shaped" spherical particles with $\rho' < 1$ fall on the trend of Figure 9.

It is important to note that another type of irregularly shaped particle, the fractal aggregate, does not fall on the trend in Figure 9. Reference [*Sorensen*, 2001] shows that the phase shift parameter $\rho \to 0$ as the aggregate size increases when $D_m < 2$. The same argument can be applied to ρ'. Furthermore, due to their fractal hence ramified nature, the internal coupling is usually weak even when D_m is larger than two. Fractal aggregates have $D_m = D_s$, to yield the well-known light scattering result that $I \sim q^{-D_m}$. Thus, a fractal aggregate can have $\rho' < 1$, but with a power law exponent much less than 4, a result not on the trend in Figure 9. We conclude that the particle types studied in this work cannot be represented by fractal morphology.

At this time, we can offer neither an explanation for the power laws found empirically above nor their behavior as a function of ρ'. However, this latter behavior is consistent with the fact that the interior field of any particle shape darkens and develops phase differences relative to the incident field due to internal coupling with increasing ρ' once $\rho' > 1$. The consequence of this is that the forward scattering lobe intensity decreases relative to Rayleigh scattering. On the other hand, the Rayleigh normalized scattering at the largest value of $qR = 2kR$ remains approximately constant as ρ' increases. This implies that the intensity difference between the forward and backward scattered light is less for larger ρ'. This conclusion is consistent with an exponent decreasing with increasing ρ'.

6. Conclusions

Q-space analysis reveals power laws with quantifiable exponents for all irregularly shaped particles, both real and simulated, studied in this survey. Furthermore, all the particles studied here display a scattering pattern consistent with Figure 1. We suggest that Figure 1 very likely represents a fundamental paradigm for scattering regimes obeyed by these particles. This rather surprising result means that the apparent complexity in shapes that these various samples represent has only a minor influence of the details of their angular scattering patterns.

The power law exponents show a universal functionality with respect to the internal coupling parameter ρ' regardless of their specific structure. The exponents start from 4, consistent with the RDG, diffraction limit, and then beginning near $\rho' \simeq 1$, decrease with increasing ρ' until the exponents reach a constant 1.75 ± 0.25 when $\rho' \gtrsim 10$. The diffraction limit exponent when $\rho' < 1$ implies that despite their irregular structures, all the particles studied here have a mass scaling dimension of $D_m = 3$ and a surface scaling dimension of $D_s = 2$. This is different from fractal aggregates that have a single power law equal to the fractal dimension D_f but with different scaling dimensions $D_f = D_m = D_s < 3$. Spheres (a "regular" shape), on the other hand, have $D_m = 3$ and $D_s = 2$ but do not show a single power law nor the same functionality with ρ'. Thus, it appears that Q-space analysis can differentiate between spheres and these two types of irregularly shaped particles. Furthermore, these observations suggest that the ill-defined terms "regular" and "irregular" might gain some resolution with these and future observations.

The ratio of forward to backscattered intensities is of critical importance to atmospheric radiative transfer calculations, as it changes the computed heating or cooling properties of layers of dust aerosols. Figures 2–4 demonstrate that laboratory data frequently do not measure at small enough q values (i.e., small enough scattering angles) to accurately determine the Guinier regime and the scattered intensity in the forward direction. This problem must be addressed in future measurements. However, until that time, Figure 1 combined with a known effective size and refractive index with which one can calculate ρ', the power law exponent determined empirically with Figure 9, and finally the position of the Guinier regime from the effective size, would allow this ratio to be calculated.

References

Berg, M. J., C. M. Sorensen, and A. Chakrabarti (2005), Patterns in Mie scattering: Evolution when normalized by the Rayleigh cross section, *Appl. Opt.*, *44*(34), 7487–7493, doi:10.1364/AO.44.007487.

Bohren, C. F., and D. R. Huffman (1998), *Absorption and Scattering of Light by Small Particles*, Wiley-VCH, Weinheim, Germany.

Curtis, D. B., B. Meland, M. Aycibin, N. P. Arnold, V. H. Grassian, M. A. Young, and P. D. Kleiber (2008), A laboratory investigation of light scattering from representative components of mineral dust aerosol at a wavelength of 550 nm, *J. Geophys. Res.*, *113*(D8), D08210, doi:10.1029/2007JD009387.

Draine, B., and P. Flatau (1994), Discrete-dipole approximation for scattering calculations, *J. Opt. Soc. Am. A*, *11*(4), 1491–1499, doi:10.1364/JOSAA.11.001491.

Dubovik, O., et al. (2006), Application of spheroid models to account for aerosol particle nonsphericity in remote sensing of desert dust, *J. Geophys. Res.*, *111*(D11), D11208, doi:10.1029/2005JD006619.

Ghan, S. J., and S. E. Schwartz (2007), Aerosol properties and processes—A path from field and laboratory measurements to global climate models, *Bull. Am. Meteorol. Soc.*, *88*(7), 1059–1083, doi:10.1175/BAMS-88-7-1059.

Gorner, P., D. Bemer, and J. F. Fabries (1995), Photometer measurement of polydisperse aerosols, *J. Aerosol Sci.*, *26*(8), 1281–1302, doi:10.1016/0021-8502(95)00049-6.

Hecht, E. (2002), *Optics*, Addison-Wesley, San Francisco, Calif.

Heinson, W. R., A. Chakrabarti, and C. M. Sorensen (2014), Crossover from spherical particle Mie scattering to circular aperture diffraction, *J. Opt. Soc. Am. A*, *31*(11), 2362–2364, doi:10.1364/JOSAA.31.002362.

Heinson, W. R., A. Chakrabarti, and C. M. Sorensen (2015), A New Parameter to Describe Light Scattering by an Arbitrary Sphere, *Opt. Commun.*, *356*, 612–615, doi:10.1016/j.optcom.2015.08.067.

Henyey, L. G., and J. L. Greenstein (1941), Diffuse radiation in the Galaxy, *Astrophys. J.*, *93*, 70–83, doi:10.1086/144246.

Hoff, R. M., and S. A. Christopher (2009), Remote sensing of particulate pollution from space: Have we reached the promised land?, *J. Air Waste Manage. Assoc.*, *59*(6), 645–675, doi:10.3155/1047-3289.59.6.645.

Kahn, R. A., and B. J. Gaitley (2015), An analysis of global aerosol type as retrieved by MISR, *J. Geophys. Res. Atmos.*, *120*, 4248–4281, doi:10.1002/2015JD023322.

Kalashnikova, O. V., and I. N. Sokolik (2004), Modeling the radiative properties of nonspherical soil-derived mineral aerosols, *J. Quant. Spectros. Radiat. Transfer*, *87*(2), 137–166, doi:10.1016/j.jqsrt.2003.12.026.

Kalashnikova, O. V., D. J. Diner, R. A. Kahn, and B. J. Gaitley (2004), *Dust Aerosol Retrieval Results From MISR*, Proc. SPIE, Fourth Intern. Asia-Pacific Environ. Remtote Sens. Symp., 8-11 Nov.

Kerker, M. (1969), *The Scattering of Light and Other Electromagnetic Radiation*, Academic Press.

Laan, E. C., H. Volten, D. M. Stam, O. Munoz, J. W. Hovenier, and T. L. Roush (2009), Scattering matrices and expansion coefficients of martian analogue palagonite particles, *Icarus*, *199*(1), 219–230, doi:10.1016/j.icarus.2008.08.011.

Lamberg, L., K. Muinonen, J. Ylonen, and K. Lumme (2001), Spectral estimation of Gaussian random circles and spheres, *J. Comput. Appl. Math.*, *136*(1–2), 109–121, doi:10.1016/S0377-0427(00)00578-1.

Maughan, J., C. Sorensen, and A. Chakrabarti (2015), Q-space analysis of light scattering from Gaussian random spheres, *J. Quant. Spectros. Radiat. Transfer*, doi:10.1016/j.jqsrt.2015.12.002.

Mie, G. (1908), Beiträge zur Optik trüber Medien, speziell kolloidaler Metallösungen, *Ann. Phys.*, *330*(3), 377–445, doi:10.1002/andp.19083300302.

Muinonen, K. (1998), Introducing the Gaussian shape hypothesis for asteroids and comets, *Astron. Astrophys.*, *332*(3), 1087–1098.

Muinonen, K., and J. S. V. Lagerros (1998), Inversion of shape statistics for small solar system bodies, *Astron. Astrophys.*, *333*(2), 753–761.

Muinonen, K., E. Zubko, J. Tyynela, Y. G. Shkuratov, and G. Videen (2007), Light scattering by Gaussian random particles with discrete-dipole approximation, *J. Quant. Spectros. Radiat. Transfer*, *106*(1–3), 360–377, doi:10.1016/j.jqsrt.2007.01.049.

Munoz, O., H. Volten, J. F. de Haan, W. Vassen, and J. W. Hovenier (2000), Experimental determination of scattering matrices of olivine and Allende meteorite particles, *Astron. Astrophys.*, *360*(2), 777–788.

Munoz, O., H. Volten, J. F. de Haan, W. Vassen, and J. W. Hovenier (2001), Experimental determination of scattering matrices of randomly oriented fly ash and clay particles at 442 and 633 nm, *J. Geophys. Res.*, *106*(D19), 22,833–22,844, doi:10.1029/2000JD000164.

Munoz, O., H. Volten, J. F. de Haan, W. Vassen, and J. W. Hovenier (2002), Experimental determination of the phase function and degree of linear polarization of El Chichon and Pinatubo volcanic ashes, *J. Geophys. Res.*, *107*(D13), 4174, doi:10.1029/2001JD000983.

Munoz, O., H. Volten, J. W. Hovenier, B. Veihelmann, W. J. van der Zande, L. Waters, and W. I. Rose (2004), Scattering matrices of volcanic ash particles of Mount St. Helens, Redoubt, and Mount Spurr Volcanoes, *J. Geophys. Res.*, *109*, D16201, doi:10.1029/2004JD004684.

Munoz, O., H. Volten, J. W. Hovenier, M. Min, Y. G. Shkuratov, J. P. Jalava, W. J. van der Zande, and L. Waters (2006), Experimental and computational study of light scattering by irregular particles with extreme refractive indices: hematite and rutile, *Astron. Astrophys.*, *446*(2), 525–535, doi:10.1051/0004-6361:20053727.

Munoz, O., H. Volten, J. W. Hovenier, T. Nousiainen, K. Muinonen, D. Guirado, F. Moreno, and L. B. F. M. Waters (2007), Scattering matrix of large Saharan dust particles: Experiments and computations, *J. Geophys. Res.*, *112*, D13215, doi:10.1029/2006JD008074.

Munoz, O., F. Moreno, D. Guirado, D. D. Dabrowska, H. Volten, and J. W. Hovenier (2012), The Amsterdam-Granada Light Scattering Database, *J. Quant. Spectros. Radiat. Transfer*, *113*(7), 565–574, doi:10.1016/j.jqsrt.2012.01.014.

Nousiainen, T., O. Munoz, H. Lindqvist, P. Mauno, and G. Videen (2011a), Light scattering by large Saharan dust particles: Comparison of modeling and experimental data for two samples, *J. Quant. Spectros. Radiat. Transfer*, *112*(3), 420–433, doi:10.1016/j.jqsrt.2010.09.003.

Nousiainen, T., H. Lindqvist, G. M. McFarquhar, and J. Um (2011b), Small irregular ice crystals in tropical cirrus, *J. Atmos. Sci.*, *68*(11), 2614–2627, doi:10.1175/2011JAS3733.1.

Oh, C., and C. M. Sorensen (1999), Scaling approach for the structure factor of a generalized system of scatterers, *J. Nanopart. Res.*, *1*(3), 369–377, doi:10.1023/A:1010033111039.

Popovicheva, O., E. Kireeva, N. Persiantseva, M. Timofeev, H. Bladt, N. P. Ivleva, R. Niessner, and J. Moldanová (2012), Microscopic characterization of individual particles from multicomponent ship exhaust, *J. Environ. Monit.*, *14*(12), 3101–3110, doi:10.1039/C2EM30338H.

Porod, G. (1951), Die Röntgenkleinwinkelstreuung von dichtgepackten kolloiden Systemen, *Kolloid-Z.*, *124*(2), 83–114, doi:10.1007/BF01512792.

Purcell, E. M., and C. R. Pennypacker (1973), Scattering and Absorption of Light by Nonspherical Dielectric Grains, *Astrophys. J.*, *186*(2), 705–714, doi:10.1086/152538.

Sorensen, C. M. (2001), Light Scattering by Fractal Aggregates: A Review, *Aerosol Sci. Technol.*, *35*(2), 648–687, doi:10.1080/02786820117868.

Sorensen, C. M. (2013a), Q-space analysis of scattering by dusts, *J. Quant. Spectros. Radiat. Transfer*, *115*, 93–95, doi:10.1016/j.jqsrt.2012.09.001.

Sorensen, C. M. (2013b), Q-space analysis of scattering by particles: A review, *J. Quant. Spectros. Radiat. Transfer*, *131*, 3–12, doi:10.1016/j.jqsrt.2012.12.029.

Sorensen, C. M., and D. J. Fischbach (2000), Patterns in Mie scattering, *Opt. Commun.*, *173*(1–6), 145–153, doi:10.1016/S0030-4018(99)00624-0.

Sorensen, C. M., E. Zubko, W. R. Heinson, and A. Chakrabarti (2014), Q-space analysis of scattering by small irregular particles, *J. Quant. Spectros. Radiat. Transfer*, *133*, 99–105, doi:10.1016/j.jqsrt.2013.07.020.

van de Hulst, H. C. (1981), *Light Scattering by Small Particles*, Reprint, edition, Dover Publ., New York.

Veihelmann, B., T. Nousiainen, M. Kahnert, and W. J. van der Zande (2006), Light scattering by small feldspar particles simulated using the Gaussian random sphere geometry, *J. Quant. Spectros. Radiat. Transfer*, *100*(1–3), 393–405, doi:10.1016/j.jqsrt.2005.11.053.

Volten, H., O. Munoz, E. Rol, J. F. de Haan, W. Vassen, J. W. Hovenier, K. Muinonen, and T. Nousiainen (2001), Scattering matrices of mineral aerosol particles at 441.6 nm and 632.8 nm, *J. Geophys. Res.*, *106*(D15), 17,375–17,401, doi:10.1029/2001JD900068.

Volten, H., O. Muñoz, J. R. Brucato, J. W. Hovenier, L. Colangeli, L. B. F. M. Waters, and W. J. van der Zande (2006), Scattering matrices and reflectance spectra of forsterite particles with different size distributions, *J. Quant. Spectros. Radiat. Transfer*, *100*(1–3), 429–436, doi:10.1016/j.jqsrt.2005.11.074.

Wang, X., G. Chancellor, J. Evenstad, J. E. Farnsworth, A. Hase, G. M. Olson, A. Sreenath, and J. K. Agarwal (2009), A Novel Optical Instrument for Estimating Size Segregated Aerosol Mass Concentration in Real Time, *Aerosol Sci. Technol.*, *43*(9), 939–950, doi:10.1080/02786820903045141.

Wang, Y., A. Chakrabarti, and C. M. Sorensen (2015), A light-scattering study of the scattering matrix elements of Arizona Road Dust, *J. Quant. Spectros. Radiat. Transfer*, *163*, 72–79, doi:10.1016/j.jqsrt.2015.05.002.

Zubko, E., Y. Shkuratov, N. N. Kiselev, and G. Videen (2006), DDA simulations of light scattering by small irregular particles with various structure, *J. Quant. Spectros. Radiat. Transfer*, *101*(3), 416–434, doi:10.1016/j.jqsrt.2006.02.055.

Zubko, E., Y. Shkuratov, M. Mishchenko, and G. Videen (2008), Light scattering in a finite multi-particle system, *J. Quant. Spectros. Radiat. Transfer*, *109*(12–13), 2195–2206, doi:10.1016/j.jqsrt.2008.03.007.

Zubko, E., H. Kimura, Y. Shkuratov, K. Muinonen, T. Yamamoto, H. Okamoto, and G. Videen (2009), Effect of absorption on light scattering by agglomerated debris particles, *J. Quant. Spectros. Radiat. Transfer*, *110*(14–16), 1741–1749, doi:10.1016/j.jqsrt.2008.12.006.